PCCP

Interactions between H-bonded [$Cu^{II}_3(\mu_3$-OH)] triangles; A combined magnetic susceptibility and EPR study.

Journal:	*Physical Chemistry Chemical Physics*
Manuscript ID	CP-ART-04-2018-002643.R1
Article Type:	Paper
Date Submitted by the Author:	04-Jun-2018
Complete List of Authors:	Mathivathanan, Logesh; Florida International University , Department of Chemistry & Biochemistry Boudalis, Athanassios; Universite de Strasbourg, Institut de Chimie Turek, Philippe; Universite de Strasbourg, Institut de Chimie, Pissas, Michael; nstitute of Advanced Materials, Physicochemical Processes, Nanotechnology and Microsystems Sanakis, Yiannis; NCSR "Demokritos", Institute of Nanoscience and Nanotechnology Raptis, Raphael; Florida International University, Chemistry and Biochemistry

Journal Name

ARTICLE

Interactions between H-bonded $[Cu^{II}_3(\mu_3\text{-OH})]$ triangles; A combined magnetic susceptibility and EPR study.

Received 00th January 20xx,
Accepted 00th January 20xx

DOI: 10.1039/x0xx00000x

www.rsc.org/

Logesh Mathivathanan,[a] Athanassios K. Boudalis,[a,b] Philippe Turek,[b] Michael Pissas,[c] Yiannis Sanakis,[c]* Raphael G. Raptis[a]*

The X-ray crystal structure of the Cu^{II} complex $[Cu_3(\mu_3\text{-OH})(\mu\text{-pz})_3(PhCOO)_3]^-$ (pz^- = pyrazolato anion) shows an isosceles triangular core, further forming a hexanuclear H-bonded aggregate. Cleavage of the H-bonds in solution results in isolated trinuclear species. Analysis of variable temperature magnetic susceptibility data of a powder sample shows an antiferromagnetically-coupled Cu_3-core with a doublet ground state and isotropic exchange parameters (J_{ave} = -355 cm^{-1}, $H_{iso} = -J_{ij}S_iS_j$). The fitting of magnetic data requires the inclusion of antisymmetric exchange, AE ($H_{AE} = \mathbf{G_{ij}} \bullet S_i x S_j$) with G_z = 31.2 cm^{-1} and no detectable *inter*-Cu_3 isotropic exchange. X-band EPR spectroscopy in a frozen tetrahydrofuran solution of the compound indicates isolated Cu_3-species with $g_{||,eff}$ = 2.25, $g_{\perp,eff}$ =1.67. The small value of $g_{\perp,eff}$ (<<2.0) is consistent with the presence of AE in agreement with the analysis of the magnetic measurements. The parallel component exhibits a hyperfine pattern corresponding to *one* I = 3/2 nucleus with $A_{||}$ = 425 MHz. This implies a specific exchange coupling scheme obeying the order $|J_{12}| = |J_{13}| < |J_{23}|$ consistent with the crystallographically determined two long and one short Cu···Cu distances. The role of AE in modulating the hyperfine parameters in antiferromagnetic Cu_3 clusters is studied. EPR spectra at X- and Q-band were performed with powder samples of the cluster at liquid helium temperatures. The spectra in both bands are consistent with two interacting $S_{a,b}$ = 1/2 species in the point dipolar approximation. Fitting of the spectra reveals that each spin is characterized by $g_{||}$ = 2.24, $g_{\perp}$ = 1.65 which is in agreement with an isolated Cu_3 cluster in the ground state. The determined *inter*-spin distance of 4.4 - 4.5 Å is very close to the distance between the Cu(1) and Cu(1)' sites of the two trimeric units as imposed crystallographically (4.3 Å). This constitutes further verification of the specific exchange coupling scheme within each trimer. Magnetostructural correlations previously adopted for antiferromagnetically coupled Cu_3 clusters are discussed in the light of the combined magnetic measurements and EPR spectroscopy.

Introduction

Magnetic interactions among metal centers in a trinuclear, triangular arrangement comprising half-integer spin ions have been of interest for a long time as their study probes fundamental questions of magnetic exchange, such as the magnitude of isotropic exchange, spin frustration and the role of antisymmetric exchange.[1–8] In addition to classical through-bond exchange, supramolecular interactions between triangular units have also been of interest in the construction of molecule-based quantum gates for quantum information processing.[9]

Trinuclear copper centers, such as those encountered in the active centers of several metalloproteins – *e.g.*, small laccase, which assists in the reduction of O_2 – are of additional interest, because of their critical role in biological processes.[5] EPR studies have been critical in elucidating the nature of the ground state and modeling the magnetic exchange scheme of multicopper oxidases.[10–13] Analysis of the EPR spectra for triangular Cu^{II}_3 systems has highlighted the fine details that allow the recognition of equilateral, isosceles and scalene magnetic geometries spectroscopically.[14–16] Such complexes are also of interest in quantum information processing, in the preparation of electrically-controlled and slow-decoherence qubits.[17–19]

In this context, triangular $Cu_3(\mu_3\text{-E})$-pyrazolates – e.g., compounds of formula $[Cu^{II}_3(\mu_3\text{-E})(\mu\text{-4-R-pz})_3X_3]^{n-}$ where E = O, OH, OCH_3; R = H, Cl, Br, NO_2, CH_3, CH(O); and X = monodentate ligand -- provide a convenient platform for the study of magnetic interactions.[2,3,20–22] The latter can be finely tuned from antiferromagnetic to ferromagnetic by controlling the acidity-basicity of the reaction mixture, which in turn determines the type of E-bridge and, consequently, the Cu-E-Cu angles: In a basic environment, the planar $[Cu^{II}_3(\mu_3\text{-O})]$-core is strongly antiferromagnetically coupled, resulting in a well-separated S = 1/2 ground state; at intermediate environments, a pyramidal $[Cu^{II}_3(\mu_3\text{-OH})]$ is moderately antiferromagnetic,

[a] Department of Chemistry and Biochemistry and the Biomolecular Science Institute, Florida International University, Miami, FL 33199, USA.
[b] Institut de Chimie de Strasbourg (UMR 7177, CNRS-Unistra), Université de Strasbourg, 4 rue Blaise Pascal, CS 90032, F-67081 Strasbourg, France.
[c] Institute of Nanoscience and Nanotechnology, NCSR "Demokritos", 15310 Aghia Paraskevi, Athens, Greece.

Electronic Supplementary Information (ESI) available: Details of powder EPR spectral simulation. See DOI: 10.1039/x0xx00000x

leading to a similar ground state; and a ferromagnetically coupled, trigonal bipyramidal $[Cu^{II}_3(\mu_3\text{-}Cl)_2]$ with a S = 3/2 ground state is reached in acidic conditions.[2,20,23] The trigonal bipyramidal $[Cu_3(\mu_3\text{-}Cl)_2]$ has been shown to be EPR-active, while the doublet ground state of $[Cu_3(\mu_3\text{-}O)]$ is EPR-silent at 77 K, attributed to fast relaxation.[20,22]

Furthermore, in a Cu_6 complex consisting of two eclipsed $Cu^{II}_3(\mu_3\text{-}O)$-units, magnetic susceptibility and density functional theory (DFT) analyses showed that the competition between the stronger intra-trimer and weaker inter-trimer exchanges result in a S = 1 ground state.[21,24]

We report here a $Cu_3(\mu_3\text{-}OH)$-pyrazolate complex having a rare intermolecular interaction through H-bonding. Interesting magnetostructural aspects are inferred by analysis of the EPR spectra. In the solid state, complex $(Et_3NH)[Cu_3(\mu_3\text{-}OH)(\mu\text{-}pz)_3(PhCOO)_3]\cdot H_2O$ (**1**) forms a dimer of trinuclear units connected by two H-bonds between carboxylate O-atoms of one unit and (μ_3-OH) protons of the other.

Experimental Methods

Solvents and reagents were purchased from Sigma-Aldrich. MeCN was used as received, acetone and toluene were distilled from drying agents according to standard procedures.[25]

Physical Measurements

The solution electronic absorption spectrum of 1 was recorded on a Varian CARY 500 Scan instrument in the 5000-40000 cm^{-1} range. ^{1}H NMR data were recorded on a Bruker AVANCE DPX-400 spectrometer in THF-d_8. Variable-temperature magnetic susceptibility measurements of 1 were carried out on powdered samples in the 2-300 K temperature range using a Quantum Design MPMS SQUID susceptometer operating under a magnetic field of 1 T and magnetization isotherms between 0 and 5 T were collected at 2, 2.5, 3 and 5 K. The diamagnetic correction was estimated from Pascal's constants. The analysis of the magnetic measurements was carried out using *Phi* 2.1.6;[26] The error-factor R is defined as $R = \Sigma(\chi_{exp} - \chi_{calc})^2 / N\chi_{exp}^2$, where N is the number of experimental points. X-band EPR spectra of complex **1** were collected with an upgraded Bruker ER-200D spectrometer equipped with an Anritsu MF76A microwave frequency counter, a Bruker 035M NMR Gaussmeter and an Oxford ESR900 cryostat. Spectra were obtained either with the perpendicular 4102ST or with the dual mode 4116DM cavities. Q-band spectra were recorded on an EMXplus spectrometer fitted with an EMX premium Q microwave bridge and an ER5106QTW microwave resonator operating in the TE_{012} mode and controlled by the Bruker Xenon software. For variable-temperature experiments, the resonator was fitted in an Oxford CF935 dynamic continuous flow cryostat. Simulations of the EPR spectra were obtained with the software SpinCount, or the EasySpin package.[27]

Synthesis of 1.

A reaction vessel was charged with $Cu(OH)_2$ (48.8 mg, 0.5 mmol, 98% stabilized Tech.), pyrazole (34.4 mg; 0.5 mmol) and Et_3N (70 µL, 0.5 mmol). Benzoic acid (122 g; 1.0 mmol) in 2 mL MeOH and 10 mL CH_3CN (or toluene) were added and the solution was stirred for 24 h. A brown solid was filtered off and the filtrate solvent was stripped under reduced pressure, resulting in a dark blue oil. The latter was re-dissolved in 10 mL MeCN and the blue solution was allowed to slowly evaporate, yielding dark-blue crystals of $(Et_3NH)[Cu_3(\mu_3\text{-}OH)(pz)_3(PhCOO)_3]\cdot H_2O$ (**1**) after two weeks; Yield = 90 mg, (60% based on Cu). Analysis calculated for $C_{36}H_{43}N_7Cu_3O_8$: C, 48.43; H, 4.86; N, 10.99 %. Found: C, 48.22; H, 4.63; N, 10.83 %. ^{1}H NMR (400 MHz, d^8-THF, ppm): 39.45 (s, $w_{1/2}$ = 105 Hz, 3H, p-Ph), 37.63 (s, $w_{1/2}$ = 147 Hz, 3H, H^4-pz), 35.98 (s, $w_{1/2}$ = 190 Hz, 6H, $H^{3,5}$-pz), 30.68 (s, $w_{1/2}$ = 244 Hz, 6H, o-Ph), 29.35 (s, $w_{1/2}$ = 130 Hz, 6H, m-Ph), 4.24 (s, $w_{1/2}$ = 66 Hz, 9H, CH_3-Et_3NH^+), 1.92 (s, $w_{1/2}$ = 28 Hz, 6H, CH_2-Et_3NH^+).

X-ray Crystallographic Data Collection and Refinement of the Structure

X-ray diffraction data for **1** were collected from a single crystal mounted atop a glass fiber with a Bruker SMART 1K CCD diffractometer. Data were corrected for Lorentz and polarization effects.[28] The structure was solved employing the *SHELX*-97 suite of programs and refined by least-squares methods on F^2 via *SHELXTL-97*, incorporated in *SHELXTL*, version 5.1 or 6.4 and with SHELXL incorporated into Olex2.[29,30]

Results and Discussion

Complex **1** forms in a one-pot reaction when $Cu(OH)_2$, PhCOOH, pzH and Et_3N are stirred in MeCN in a 1:2:1:2 ratio. Crystals of **1** are soluble in THF or acetone and insoluble in MeCN or CH_2Cl_2. The ^{1}H-NMR spectrum of freshly prepared THF solution of **1** shows broad, paramagnetically shifted singlet resonances of the benzoate and pyrazolate protons, as expected (Fig. 1). Furthermore, the width at half-height, $w_{1/2}$, of the phenyl group resonances follows the order o- > m- > p-, reflecting the decreasing transverse relaxation time, T_2, of protons further away from the paramagnetic metal center. However, after approximately 20 minutes, the three benzoate

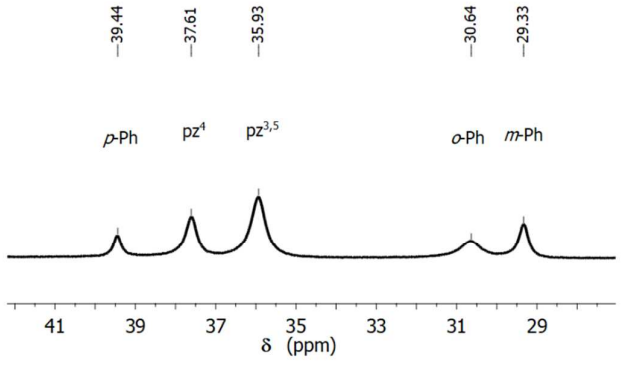

Fig. 1. ^{1}H-NMR of **1** showing the paramagnetically shifted and broadened resonances of pyrazole and phenyl protons.

resonances appear between 8.55, 7.87 and 7.35 ppm for *o*-, *m*- and *p*-Ph protons, respectively, with no paramagnetic broadening, while the pyrazolate protons remain paramagnetically shifted. The same behavior is observed in d^8-DMSO. This is a clear indication that the benzoate ligands dissociate in coordinating solvents (*vide infra*).

The crystal structure of $(Et_3NH)[Cu_3(\mu_3\text{-}OH)(\mu\text{-}pz)_3(PhCOO)_3]\cdot H_2O$ (**1**) including all H-bonds is shown in Fig. 2. Its unit cell consists of two Cu_3 units related by a crystallographic inversion center. Bond distances and angles within the trinuclear units are similar to other $[Cu_3(\mu_3\text{-}OH)]$-complexes reported.[6,22,23,31–33] The Cu–OH bonds are 1.968(2), 1.978(5) and 2.008(2) Å long, while the the Cu–N bonds fall in the range of 1.928(2) – 1.953(3) Å. The capping μ_3–OH^- is located 0.524 Å away from the Cu_3-plane, forcing a trigonal pyramidal geometry on the $[Cu_3(\mu_3\text{-}OH)]$-core. Compound **1** has three monodentate benzoate ligands with average Cu-O of 1.970(2) Å. The three bridging pyrazolate ligands are coplanar with the Cu_3-plane. All Cu-centers are in a square planar N_2O_2 coordination environment with the normal to the CuN_2O_2 best-fit planes forming angles of 29.14º, 30.14º and 36.86º. The carboxylic oxygen atoms are unsymmetrically arranged with respect to the μ_3-OH cap: two are *anti* and one is *syn* to μ_3-OH. The carboxylate *syn* to the cap is involved in an H-bond with the μ_3-OH cap of the adjacent trinuclear complex, forming a dimer connected by a pair of H-bonds. Carboxylic oxygen atoms *anti* to the μ_3-OH cap form one H-bond each with the interstitial water molecule and one with the $(Et_3NH)^+$ counter cation. The shortest inter-trimer Cu···Cu distance is 4.3338(7) Å.

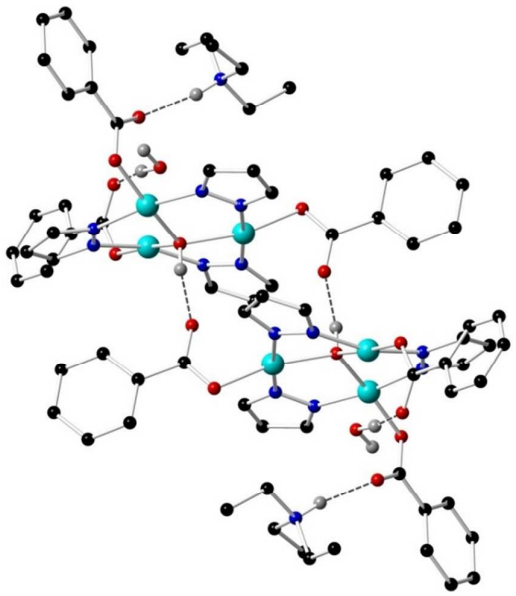

Fig. 2. Molecular structure of **1** (CCDC 1557913) showing four different types of H-bonds. Color codes: cyan, Cu; blue, N; red, O; black, C; gray, H. Carbonic H-atoms are not shown for clarity.

Pyrazolato complexes with a $[Cu_3(\mu_3\text{-}OH)]$ core are fairly common. Several groups have reported a variety of complexes similar to **1** with various terminal ligands.[6,23,32,34,35] For example, reactions of a carboxylic acid with a Cu(II) salt and pyrazole usually yield complexes with $[Cu_3(\mu_3\text{-}OH)]$-core and carboxylate terminal ligands (i.e., $[Cu_3(\mu_3\text{-}OH)(\mu\text{-}pz)_3(OCOR)_3]^-$).[34] Extensive structural, catalytic and reactivity studies of such complexes, as well as polymeric materials based on Cu_3-pyrazolate units have been reported.[34] However, their EPR studies have been scarce, owing to the fact that the spectra are ill-resolved at room temperature.[33,36,37] Three relevant papers have reported that magnetic exchange interactions through inter/intramolecular H-bonds are either negligible or small.[38–40]

Magnetic Properties

At 300 K, the $\chi_M T$ value of **1** (1 T) is 0.53 $cm^3\ mol^{-1}$ K, significantly below the theoretically expected value for three non-interacting S = 1/2 ions (1.13 $cm^3\ mol^{-1}$ K, g = 2), indicating strong antiferromagnetic interactions (Fig. 3). This conclusion is further corroborated by the rapid decrease of the $\chi_M T$ value upon cooling, reaching a plateau of ~0.40 $cm^3\ mol^{-1}$ K at approximately 100 K, then resuming its decrease, reaching a value of 0.35 $cm^3\ mol^{-1}$ K at 2 K. An initial model considering a single isotropic exchange interaction (equilateral magnetic symmetry) was taken into account in order to obtain an estimate for the magnitude of the exchange coupling constants within the framework of the Hamiltonian (Eq. 1): Table 1. Crystallographic Data for **1**.

Chemical formula	$C_{36}H_{43}Cu_3N_7O_8$
Formula weight	892.39
Temperature	296 K
Wavelength	0.71073 Å
Crystal system	Triclinic
Space group	$P\ \bar{1}$
Unit cell dimensions	a = 11.417 (2) Å; α = 73.446(2)°
	b = 12.317 (3) Å; β = 79.252(2)°
	c = 15.889 (3) Å; γ = 65.891(2)°
Volume	1948.7(7) $Å^3$
Z	2
Density (calculated)	1.521 mg/m^3
Absorption coeff.	1.681 mm^{-1}
F (000)	918
Crystal size	0.14 x 0.09 x 0.08 mm^3
θ range	1.96 to 27.56°.
Reflections collected	22341
Independent refl.	8671 [R(int) = 0.024]
Completeness	99.7 % (to theta 25.00°)
Abs. correction	SADABS
Min. and max. T	0.690, 0.746
Data/restr./param.	8672/ 2 / 506
Goodness-of-fit on F^2	0.997
Final R [I>2σ(I)]	R_1 = 0.0314, wR_2 = 0.0776
R indices (all data)	R_1 = 0.0505, wR_2 = 0.0867
Largest peak and hole	0.30 and -0.31e.$Å^{-3}$

$$\hat{H}_{eq} = -J_{eq}\sum_{i,j}\hat{\mathbf{S}}_i\hat{\mathbf{S}}_j + \beta g\mathbf{H}\sum_{i=1}^{3}\hat{\mathbf{S}}_i \qquad \text{(Eq. 1)}$$

This model, predicts two S = 1/2 low-lying degenerate states. Within this model, the data for T > 150 K can be reproduced with J_{eq} = -344 cm^{-1} and g = 2.070 (Fig. S1). At low temperatures, only the two low-lying states should be occupied and χ_MT should be temperature independent with a value of ~0.41 cm^3 mol^{-1} K. At sufficiently low temperatures, magnetic field effects should lead to deviations from the Curie approximation, causing a rather steep drop of $\chi_M T$. However, this model clearly fails to account for the temperature dependence of $\chi_M T$ below 100 K (Fig. S1).

On the basis of the crystal structure of **1** (Fig. 2), it is necessary to examine whether the behavior at the low temperature regime is governed by magnetic interactions between the two neighboring triangular units, mediated by H-bonding. In order to account for the decrease of $\chi_M T$ below 170 K, these interactions should be antiferromagnetic. Qualitatively, below 170 K, only the S = 1/2 states of the trimers are occupied and the system can be described as comprising two antiferromagnetically coupled entities, *a* and *b,* each with effective spin $S_a = S_b$= 1/2 through an isotropic exchange constant J_{ab} (<0). In this case, the ground state is diamagnetic, with the next excited state having a S_{ab} = 1. The value of $\chi_M T$ at low temperatures depends on the occupation of states with non-zero spin. In the present case, the value of $\chi_M T$ = 0.35 cm^3 mol^{-1} K at 2.0 K (or 0.70 cm^3 mol^{-1} K, if we consider the dimer of clusters) is indicative of significant occupation of the S_{ab} = 1 excited state, further suggesting that J_{ab} cannot be much larger than a few cm^{-1}.

On the basis of the relative arrangement of the triangles in **1** (Scheme 1), weak Cu(1)/Cu(1') interactions are taken into account; the longer range Cu(2)/Cu(3) and Cu(2')/Cu(3') interactions are neglected in this approximation. In this case the relevant exchange Hamiltonian becomes (Eq. 2):

$$\hat{H}_{eq} = -J_{\text{intra}}\left[\sum_{i,j=1,2,3}\hat{\mathbf{S}}_i\hat{\mathbf{S}}_j + \sum_{i,j=1',2',3'}\hat{\mathbf{S}}_i\hat{\mathbf{S}}_j\right] - J_{\text{inter}}\hat{\mathbf{S}}_1\hat{\mathbf{S}}_{1'} + \beta g\mathbf{H}\sum_{i=1}^{6}\hat{\mathbf{S}}_i \qquad \text{(Eq. 2)}$$

In equation 2, the second term describes the *inter*-triangle interactions and is expected to be much smaller than the first term, which relates to the *intra*-triangle interactions. Representative simulations are included in Fig. 3 for indicative values of J_{intra} = -320 cm^{-1}, J_{inter} ~ -2.5 cm^{-1} and g = 2.04, with $\chi_M T$ values scaled for a single Cu_3 cluster. This model predicts a wide plateau and a rather steep decrease of $\chi_M T$ at low temperatures and cannot account for the observed behavior.

The above analysis indicates that (a) H-bond-mediated superexchange between the triangular units is negligible, at least as far as magnetic susceptometry is concerned, and (b) that the magnetic behavior of **1** should be modulated by other mechanisms. Similar behavior of the $\chi_M T$ *vs*. T data has been observed in several antiferromagnetically coupled trinuclear clusters.[2,3,8,41–45]

It has been demonstrated that the low-lying doublets of antiferromagnetically coupled half-integer spin triangles are non-degenerate, a property that is also referred to as "magnetic Jahn-Teller effect".[46] Usually, this non-degeneracy is rationalized by considering a decrease of the magnetic symmetry and/or the inclusion of an antisymmetric exchange term, characterized by a vector **G**.[4,47–51] Whereas a dynamic mechanism has been recently proposed for the lifting of the degeneracy through isotropic interactions in highly symmetric triangles without a lowering of their symmetry,[52] static distortions provide a valid model for less symmetric triangles such as **1**. Symmetry-lowering of the isotropic interactions was unsuccessful in fitting the experimental data (Fig. S1). Subsequently, the case of both mechanisms operating in tandem was considered, corresponding to the Hamiltonian in Eq. 3.

$$\hat{H}_{anti} = -J_{12}\hat{\mathbf{S}}_1\hat{\mathbf{S}}_2 - J_{13}\hat{\mathbf{S}}_1\hat{\mathbf{S}}_3 - J_{23}\hat{\mathbf{S}}_2\hat{\mathbf{S}}_3 + \mathbf{G}\cdot(\hat{\mathbf{S}}_1\times\hat{\mathbf{S}}_2 + \hat{\mathbf{S}}_2\times\hat{\mathbf{S}}_3 + \hat{\mathbf{S}}_3\times\hat{\mathbf{S}}_1) + \beta\mathbf{H}\sum_{i=1}^{3}\hat{g}_i\hat{\mathbf{S}}_i \qquad \text{(Eq. 3)}$$

In order to avoid overparametrization, an isosceles model with $J_{12} = J_{13} = J$, and $J_{23} = j$ and with a common isotropic g value for the g_i-tensors of the individual Cu ions was adopted, considering also that the **G** vector is perpendicular to the Cu_3-plane, i.e. $G_z >> (G_x, G_y) \sim 0$. Simultaneous χ_MT *vs.* T and *M vs. H* fits according to this model yield two best-fit solutions, one with $|J| > |j|$ and one with $|J| < |j|$. These are: J = -392 cm^{-1}, j = -278 cm^{-1} (solution **A**) and J = -316 cm^{-1}, j = -432 cm^{-1} (solution **B**); for both solutions the remaining parameters and agreement factors are practically identical, with G_z = 31.2 cm^{-1}, g = 2.096 and R = 2.5×10^{-4}. For both solutions the average exchange coupling $J_{ave} = (2J+j)/3$ = -355 cm^{-1} and the difference

Scheme 1. Spin-coupling scheme for **1**. Full arrows indicate superexchange interactions. The dashed arrow indicates a dipolar interaction (see text).

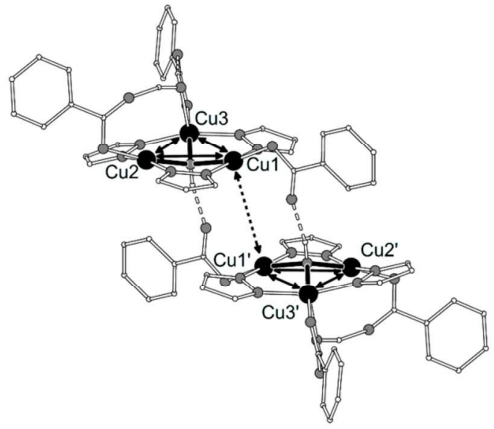

Table 2. Selected interatomic distances (Å) in **1**.

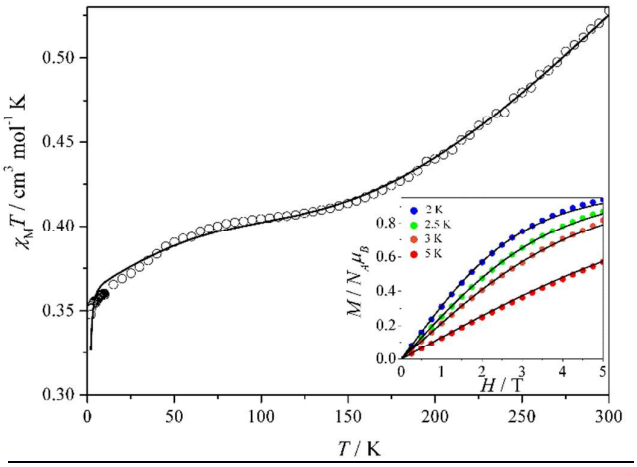

Cu(1)-Cu(2)	3.3500(8)	Cu(2)-Cu(3)	3.2440(8)
Cu(1)-Cu(3)	3.3519(7)		
Cu(1)-O(1)	1.978(2)	Cu(1)-N(1)	1.953(3)
Cu(2)-O(1)	1.968(2)	Cu(1)-N(6)	1.939(3)
Cu(3)-O(1)	2.008(2)	Cu(2)-N(2)	1.932(2)
Cu(1)-O(2)	1.974(2)	Cu(2)-N(3)	1.928(2)
Cu(2)-O(4)	1.966(2)	Cu(3)-N(4)	1.950(2)
Cu(3)-O(6)	1.970(2)	Cu(3)-N(5)	1.945(2)
O(1)…O(3)	2.639(2)	O(3)…O(8)	2.902(4)
O(5)…N(7)	2.822(3)	O(7)…O(8)	2.674(4)

Fig. 3. χ_MT *vs.* T and *M vs.*H (inset) experimental data and calculated curves (solid lines) for **1**, as described in the text.

between the two constants is $\delta = |J - j| \sim$ -115 cm^{-1}. The existence of two different sets of parameters that reproduce the magnetic susceptibility data of antiferromagnetic trinuclear clusters comprising half-integer spin ions had been recognized earlier.[53] In the case of triangles comprising S = 1/2 metal ions, the two low-lying doublets (S_T = 1/2) are separated by the quantity δ and the excited quartet's (S_T = 3/2) energy only depends on J_{ave}. Since neither δ nor J_{ave} depend on model **A** or **B**, the two fitting models should give exactly the same values for J_{ave}, δ, g, G_z and the same R factor. Any difference observed in these values is entirely due to the numerical nature of the fitting procedure.

Fig. S1 shows best-fit curves corresponding to two equilateral models (isolated and interacting triangles), as well as calculated curves based on solutions **A** and **B** with G_z = 0, illustrating the effect of antisymmetric exchange on the low-temperature magnetic behavior. These alternative models serve to justify the proposed solution involving *both* low magnetic symmetry (i.e. $J \neq j$) and antisymmetric exchange terms.

The magnetization data can be satisfactorily modeled within this framework with a common set of parameters (Fig. 3). In particular, the magnetization tends to a saturation value of 0.94 $N_A\mu_B$ at 2.0 K, smaller than the expected one for an S = 1/2 system with g_{iso} = 2.1 (0.99 $N_A\mu_B$ at 2.0 K). It is well known that under the influence of antisymmetric exchange in trinuclear systems comprising half-integer spin ions, the ground S = 1/2 state is characterized by an axial **g**-tensor with $g_\perp < g_{iso}$ (*vide infra*).[4,47–50] Accordingly, here the low saturation value of the magnetization of **1** at 2.0 K is attributed to the anisotropy of the ground state, which is further corroborated by the EPR data.

Finally, it should be mentioned that this model reproduces the low temperature isothermal magnetization data without the requirement of *inter*-cluster superexchange interactions. Actually, the model proposed here is quite sensitive to interactions between Cu(1) and Cu(1'); simulations considering best-fit solution **B** and adding a $J_{11'}$ interaction deviate significantly from the experimental data for interactions stronger than -0.4 to -0.6 cm^{-1}. Therefore, even if such interactions are operative, they cannot be stronger that -0.4 cm^{-1}.

EPR spectroscopy

a. Frozen Solution

EPR spectroscopy in a freshly prepared frozen tetrahydrofuran (THF) solution (Fig. 4) and in powder samples (Fig. 5) has been applied in order to further probe the magnetic properties of **1**.

The 4.2 K THF frozen solution spectrum consists of an absorption peak split by four hyperfine lines at g = 2.25 and a broad derivative feature extending at high field. Its temperature dependence indicates that it arises from a ground state (Fig. S2). The signal is consistent with a S = 1/2 system exhibiting axial anisotropy with $g_{||,eff}$ = 2.25 and $g_{\perp eff}$ << 2.0. The observation of a four-line hyperfine splitting at $g_{||,eff}$ suggests the involvement of one $^{63/65}$Cu nucleus with I = 3/2. However, the fact that $g_{\perp,eff}$ << 2.0 excludes the possibility that the signal arises from a monomeric Cu^{II} species. The spectrum can be simulated assuming an effective S = 1/2 spin Hamiltonian: $\hat{H}_{eff} = \beta g_{eff}\hat{S} + \hat{I}A\hat{S}$, with $g_{||,eff}$ = 2.25, $g_{\perp,eff}$ = 1.67, $A_{||}$ = 425 MHz and $A_\perp$ = 0 (the $A_\perp$ component of the hyperfine tensor is too small to be resolved in EPR spectra and was set to 0 in spectra simulations, in order to avoid overparameterization). To account for the linewidth, a distribution in the $g_{\perp,eff}$ part with $\sigma g_{\perp,eff}$ = 0.18 and an intrinsic linewidth of 4.5 mT were employed.

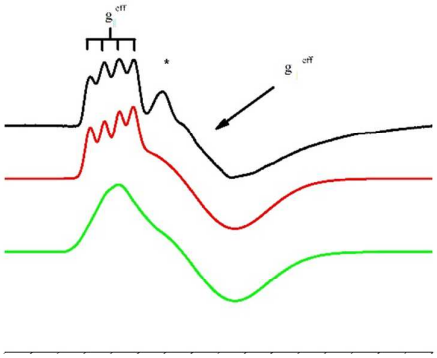

Fig. 4. X-band EPR spectra of a frozen solution in THF of **1** at 4.2 K. Black line, experimental; red line, theoretical according to model II; green line, simulated spectrum according to model I (see text for details). EPR conditions:microwave frequency, 9.41 GHz; microwave power, 0.7 μW; modulation amplitude, 10 Gpp.

This behavior is consistent with an antiferromagnetically coupled trinuclear cluster comprising half-integer spin ions in accord with the THF solution ^{1}H-NMR data (*vide supra*) with the involvement of antisymmetric exchange, but free of intermolecular interactions. The effect of antisymmetric exchange in the EPR properties of the ground S = 1/2 state for such clusters has been well documented in the literature.[3,47–51] Briefly, antisymmetric exchange induces an effective anisotropy in the g-tensor of the ground state. At X-band, the EPR spectra are characterized by an absorption peak at $g_{||,\mathrm{eff}}$ and a derivative feature corresponding to $g_{\perp\mathrm{eff}}$ given by the relationships:

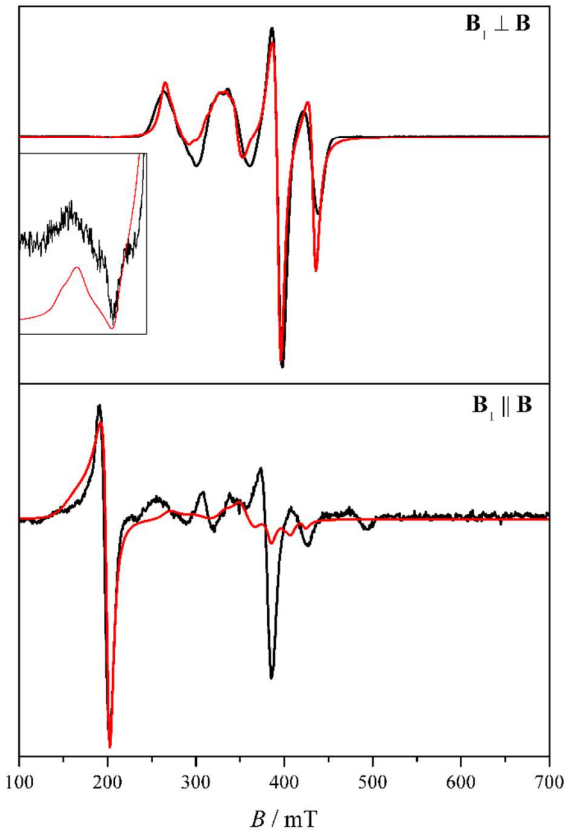

Fig. 5. Experimental (black lines) and theoretical (red lines) dual-mode powder X-band EPR spectra of **1** at 4.2 K. The trace in the inset of the perpendicular mode spectrum shows a feature associated with forbidden transitions. EPR conditions: Perpendicular mode: microwave frequency, 9.61 GHz; microwave power, 1.0 mW; modulation amplitude, 1.0 G_{pp}. Parallel mode: microwave frequency, 9.36 GHz; microwave power, 32.0 mW; modulation amplitude, 10 G_{pp}

$$g_{||,\mathrm{eff}} = g_{0||}$$

$$g_{\perp,eff} = g_{0\perp}\sqrt{\frac{\delta^2-(h\nu)^2}{\Delta^2-(h\nu)^2}},$$

with

$$\Delta = \sqrt{\delta^2 + 3G_z^2}$$

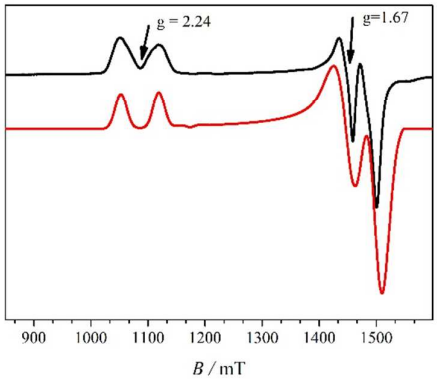

Fig. 6. Experimental (black line) and theoretical (red line) Q-band EPR powder spectra of **1** at 10 K. Experimental conditions: microwave frequency, 34.0 GHz; microwave power, 0.06 mW; modulation amplitude, 2 G_{pp}.

and $\delta = |J - j|$. $g_{0||}$, $g_{0\perp}$ are the components of the intrinsic g-tensor of the individual ions. Within this description, the absorption peak at g_{eff}=2.25 is attributed to the $g_{||}$ and the broad derivative feature to the $g_{\perp,\mathrm{eff}}$ of the trinuclear cluster. The $g_{\perp,\mathrm{eff}}$ part comprises a significantly broad derivative feature. Such characteristics are often observed in powder or frozen solution samples of antiferromagnetically coupled trinuclear clusters comprising Fe^{III} (S = 5/2),[47,48,54–57] and Cr^{III} (S = 3/2) clusters.[48,58] The particular line shape is attributed to the extreme sensitivity of $g_{\perp,\mathrm{eff}}$ on the parameters δ and Δ, as it is imposed by the equations above. Small distributions on the exchange parameters lead to significant distributions on the $g_{\perp,\mathrm{eff}}$ resulting in the observed broad high-field tail. In the present case, we assume a simple Gaussian distribution on the $g_{\perp,\mathrm{eff}}$, which accounts for the major behavior of the spectrum. A feature denoted by an asterisk in Fig. 4 is not reproduced, suggesting that a more complicated distribution scheme[49] might apply. From the g_{eff}-values for the S =1/2 ground state, a value of 1.99 is derived for the intrinsic g_{iso} values for the individual Cu ions. The discrepancy between this value and the one used for the analysis of the magnetic data (2.10) reflects the extreme sensitivity of the spectroscopic parameters on the exchange coupling constants and antisymmetric exchange.

Due to the involvement of three $^{63/65}$Cu (I = 3/2) nuclei, the EPR spectrum will be governed by the hyperfine interactions for each Cu ion. In the exchange-coupled system, the hyperfine tensors are given by Eq. 4:

$$\mathbf{A}_i = K_i\mathbf{a}_i \qquad \text{(Eq. 4)}$$

where, $\mathbf{a}_i$ is the intrinsic hyperfine tensor of each individual ion. In the present case, the similarity in the first coordination sphere of the three ions suggests that the intrinsic hyperfine tensors are equal, $\mathbf{a}_i = \mathbf{a}$. K_i is a coefficient related to the spin projection on each individual ion. This parameter depends on the nature of the ground state, which, in the isosceles configuration in the absence of antisymmetric exchange, can be expressed as $|(S_2S_3)S_{23},S_1;S,M_S\rangle$. In this notation, spins S_2 and S_3 couple to yield an intermediate spin S_{23}, which subsequently couples with S_1 to yield the total spin S. The two S = 1/2 states

can be either|(1/2,1/2)1,1/2;1/2,-1/2> (I) or |(1/2,1/2)0,1/2;1/2,-1/2> (II).

Qualitatively, the two cases can be understood as follows: In case I, the antiferromagnetic coupling in the pairs [Cu(1), Cu(2)] and [Cu(1), Cu(3)] forces Cu(2) and Cu(3) to align antiparallel with Cu(1). In this case Cu(2) and Cu(3) align parallel to each other, yielding S_{23} = 1. The latter couples antiferromagnetically to Cu(1) leading to an S = 1/2 ground state. In case II, the exchange coupling between Cu(2) and Cu(3) forces them to align antiparallel, yielding S_{23} = 0. Eventually, the cluster behaves as an isolated Cu ion (Cu(1)). Case I corresponds to$|J|>|j|$ (solution **A**), whereas case II to $|J|<|j|$ (solution **B**).

The coefficients K_i and the hyperfine tensors for the individual ions for each case I and II can be calculated using standard techniques, as follows:[14,59]

I: $\mathbf{A}_1 = -\mathbf{a}/3$, $\mathbf{A}_2 = \mathbf{A}_3 = +2\mathbf{a}/3$ (Eq. 5)

II: $\mathbf{A}_1 = \mathbf{a}$, $\mathbf{A}_2 = \mathbf{A}_3 = 0$ (Eq. 6)

For Cu ions in square planar geometry, the intrinsic hyperfine tensor $\mathbf{a}_i$ is axial with a very small perpendicular component $a_\perp$. Therefore, only the parallel $a_{||}$ component should be taken into account, whereas the $g_{\perp,\text{eff}}$ will not exhibit any observable hyperfine splitting. In case I, the spectrum should give rise to a 16-line pattern with a relative ratio of 1:1:3:3:5:5:7:7:7:7:5:5:3:3:1:1.[14] The spacing between consecutive lines will be $a/3$. In case II, the hyperfine pattern should consist of four lines with equal intensity with a spacing of a. Theoretical spectra corresponding to the two different models focusing on the $g_{||}$ region are shown in Fig. S3. Therefore, the observation of four strong lines in the experimental spectrum (Fig. 4) excludes case I and is consistent with a ground state doublet described by case II with $A_{||}$ = 425 MHz. An example of a (linear) Cu_3 system with a $|S_{23},S_T>$ = |1,1/2> ground state showing more than four lines in its EPR spectrum at Q-band has been reported.[60]

In the previous discussion, the effect of the antisymmetric exchange term has not been considered. This term mixes the two lowest S = 1/2 states[50] and the wavefunctions become linear combinations of these states, |(1/2,1/2)0,1/2,1/2,-1/2> and |(1/2,1/2)1,1/2;1/2,-1/2>. The modified K_i coefficients in the parallel direction are calculated from the relevant wavefunctions[50] and for the two cases I and II are given by the relationships:

I. $K_1 = \frac{1}{3} - \frac{2\delta}{3\Delta}$, (Eq. 7); $K_2 = K_3 = \frac{1}{3}\left(1 + \frac{\delta}{\Delta}\right)$ (Eq. 8)

II. $K_1 = \frac{1}{3} + \frac{2\delta}{3\Delta}$, (Eq. 9); $K_2 = K_3 = \frac{1}{3}\left(1 - \frac{\delta}{\Delta}\right)$ (Eq. 10)

On the basis of the values of δ and Δ determined by the analysis of the magnetic susceptibility data, the effective hyperfine tensors are given by:

I: $A_{1||} = -0.269a_{||}$, $A_{2||} = A_{3||} = 0.635a_{||}$

II: $A_{1||} = 0.936a_{||}$, $A_{2||} = A_{3||} = 0.032a_{||}$

As before, the experimental spectra are reproduced only with model II. In this model, for one site (Cu1) the hyperfine value is relatively large resulting in the four-line pattern. Accordingly, for $A_{1||}$ = 425 MHz the calculated values by Eq. 9 and Eq. 10 are for $a_{||}$ = 453 MHz and $A_{2||} = A_{3||}$ = 14.0 MHz. Because the values of $A_{2||}$ and $A_{3||}$ are much smaller than $A_{1||}$ and each of the four lines should split in seven lines (due to the effect of the other two hyperfine tensors), the overall effect is an unresolved broadening of the four strong hyperfine lines. Corroborating these results, the set of $g_{0||}$ and $a_{||}$ determined here for complex **1** fall within the expected range for a Cu^{2+} center in a square planar geometry comprising N_2O_2 chromophores.[61]

Finally, Fig. 4 includes also a simulated spectrum within the assumptions of model I. Assuming $a_{||}$ = 453 MHz, the derived values for $A_{1||}$ = 121. 9 MHz and $A_{2||} = A_{3||}$ = 287.7 MHz should cause a breakdown of the simplified 16-line pattern (anticipated in the absence of antisymmetric exchange) and give rise to 28 lines with a rather irregular spacing. For the same linewidth as in case II, the resulting simulated spectrum does not exhibit resolved hyperfine lines at $g_{||\text{eff}}$ and clearly does not match the experimental one.

While the magnitude of magnetic asymmetry, ΔJ = J - j, in this system can be nicely quantified by magnetic susceptometry, its sign cannot be determined by such study. The same holds true for EPR spectroscopic studies in the absence of hyperfine interactions, as the position of g_|_ is a function of |ΔJ| and insensitive to its sign. Other physical measurements (neutron scattering, NMR, heat capacity, etc.) can also allow the determination of the Δ gap between the low-lying doublets and, consequently, the magnetic asymmetry ΔJ, but they can be similarly insensitive to its sign. The presence of hyperfine interactions provides a mechanism through which this subtle effect is enhanced and readily distinguished. In a sense, hyperfine interactions act as an "amplifier" to the subtle magnetic effects caused by magnetic asymmetries, and increases the diagnostic power of EPR.

b. Solid Powder

Fig. 5 shows the perpendicular and parallel mode X-band EPR spectra from a powder sample of **1** recorded at 4.2 K. Clearly, the spectra do not show the characteristic S = 1/2 signals with the g-anisotropy observed in frozen solution. The spectrum comprises four strong signals in the 200 - 450 mT field region. A closer examination indicates also the presence of a weaker signal at ~190 mT (Fig. 5, inset). This set of signals is reminiscent of resonances usually observed in "triplet states" under the influence of zero-field splitting of relatively small magnitude. Specifically, the four strong signals can be attributed to the $\Delta M_S = \pm 1$ allowed transitions. The two lower field and the two higher field signals arise from the parallel and perpendicular transitions respectively (Fig. S4). The weaker signal at lower field is attributed to the forbidden, "half-field" transition ($\Delta M_S = \pm 2$). In order to confirm this assignment a spectrum was also recorded in parallel mode (Fig. 5). Under these conditions, the allowed transitions are suppressed, whereas the forbidden transitions survive, as it has been

reported for the much simpler case of Cu dimers.[62–64] Indeed, in the parallel-mode spectrum one characteristic derivative-like signal is observed at a position corresponding to the assumed forbidden transition.

Fig. 6 shows the Q-band EPR spectrum recorded from a powder sample of **1** at 10 K. The spectrum is characterized by two features centered at *ca.* 1080 mT (g_{eff}~ 2.24) and two features at *ca.* 1460 mT (g_{eff} ~ 1.67). The signals are attributed to transitions arising from an effective S = 1 system with $g_{||} > g_{\perp}$ under the influence of zero-field splitting (zfs) with a small magnitude for D parameter relative to the Zeeman term (~1.13 cm^{-1} at Q-band). Under these conditions, the splitting at $g_{||}$ relates to the effective zfs as $2D/\beta g_{||}$. Therefore, for a splitting of ~630 G, D is estimated at ~0.033 cm^{-1}.

In order to interpret the EPR spectroscopic properties from the powder sample of **1**, interactions between the neighboring hydrogen-bonded trinuclear units should be taken into account. The magnetic susceptiptibility and magnetization studies, detailed in the previous section, preclude the possibility of isotropic exchange intereactions that would lead to a real S = 1 low-lying state. On the other hand, the most plausible mechanism is through point dipolar interactions. From the estimated zfs value (above), the distance between the dipoles, r_{ab}, is derived from the relationship $|D| = 0.433g^2/r_{ab}^3$: for g ~ 2.1, r_{ab} ~ 4.0 Å.[59] More accurate values are obtained through simulations using the dipolar Hamiltonian:

$$\hat{H}_{dip} = \frac{1}{r_{ab}^3}\left[\boldsymbol{\mu_a}\cdot\boldsymbol{\mu_b} - \frac{3(\boldsymbol{\mu_a}\cdot\boldsymbol{r_{ab}})(\boldsymbol{\mu_b}\cdot\boldsymbol{r_{ab}})}{r_{ab}^2}\right], \qquad \text{(Eq. 11)}$$

where $\boldsymbol{\mu_{a,b}} = -\beta\mathbf{g_{a,b}}\boldsymbol{S_{a,b}}$

Each trinuclear unit is assumed to have an effective $S_{a,b}$ = 1/2 with anisotropic axial **g** tensor with $\mathbf{g_{ab}} = \mathbf{g_a} = \mathbf{g_b}$.[65,66] The transitions from this system are shown in Fig. S5 and coincide with those of the effective S = 1 approximation (Fig. S4) for appropriate values of the relevant parameters. The simulations shown in Fig. 5 for the X-band dual mode spectra were obtained for: $g_{ab||}$ = 2.25(1), $g_{ab\perp}$=1.66(1) and r_{ab} = 4.5(2) Å. For the Q-band (Fig. 6) the simulations yield $g_{ab||}$ = 2.24(2), $g_{ab\perp}$ = 1.64(2) and r_{ab} = 4.4(2) Å [see Supporting Information].

The obtained values for the g tensors are in good agreement with those determined by the analysis of the frozen solution X-band EPR spectrum. This is a robust evidence that in the solid state the EPR properties involve the dipolar interactions between the trinuclear units. Moreover, the fact that in frozen solution there is no evidence for intermolecular interactions and the X-band EPR spectrum can be described assuming an isolated trimer indicates that the hydrogen bonding is disrupted in solution, in agreement also with the ^{1}H-NMR data that indicate dissociation of the benzoate ligands after a few minutes in a THF solution.

It has been established that the distances derived from the analysis of EPR spectra in the point dipolar model approximation when polynuclear transition metal clusters are involved should be considered with caution.[67,68] In particular, because the unpaired spin is usually delocalized over the ions of the clusters, the distance determined by the analysis of the EPR spectra is an effective parameter and its correlation with actual geometrical elements of the system is not obvious. This problem has been studied in the case of polynuclear clusters interacting with a radical,[67] or with a single metallic center.[68] In these cases, the point approximation is quite valid for the second species and the analysis is much simpler. In our case, however, both spin systems comprise trinuclear clusters and the situation is more complex. The analysis of the frozen solution EPR spectra indicated that in the ground state the spin density is mainly located at the Cu(1) sites of the trimers with little spin density on the Cu(2) and Cu(3) sites. Therefore, the point-dipolar model will be dominated mainly by the relative arrangement of the Cu(1) sites of the trimers. An inspection of the crystal structure of **1** reveals that the relative orientations of the trimers in the dimeric aggregate is such that the distance between the Cu(1) ions is 4.3 Å (Scheme 1), while their **g**-tensors are antiparallel. Therefore, the determined distance on the basis of the dipolar model is in fair agreement with the crystal structure if the Cu(1)-Cu'(1) distance is taken into account.

Discussion – Conclusions

We report here the crystal structure and characterization of a new Cu_3-pyrazolate complex, which forms dimeric H-bonded aggregates in the solid state. Magnetic susceptometry studies revealed that the magnetic properties of each Cu_3-triangle are governed by antiferromagnetic interactions modulated by significant contributions of antisymmetric exchange. X-band EPR spectra in solution revealed hyperfine interactions compatible with a magnetic symmetry causing almost all uncoupled spin density to reside on a single center, implying an isosceles magnetic geometry with two weak and one strong interactions ($|J| < |j|$). As far as intermolecular magnetic interactions are concerned, these were indiscernible by magnetic susceptometry. However, powder X- and Q-band EPR spectroscopy revealed weak intermolecular magnetic coupling, weak enough as not to alter the basic properties of the individual magnetic triangles, but strong enough as to produce a small magnetic anisotropy through dipolar interactions. The magnitude of those interactions is such that it is perfectly compatible with the Cu(1)···Cu(1') interatomic separation, in agreement with a magnetic geometry where all spin density resides on those two centres, which is the case for two weak and one strong interactions ($|J| < |j|$). This finding is in agreement with the solution EPR data, meaning that the magnetic symmetry is retained in solution.

The relative magnitude of the isotropic exchange coupling constants between the copper ions in trinuclear $Cu_3(\mu_3\text{-OH})$ clusters has been correlated to structural features, specifically to the Cu-O(H)-Cu angles.[3] According to these magnetostructural correlations, the more obtuse angle is related with the largest (more antiferromagnetic) exchange coupling constant. Experimental verification of these magnetostructural correlations cannot be achieved by the conventional magnetic susceptibility measurements but EPR

spectroscopy is an appropriate method toward this end, employing hyperfine interactions as an amplification mechanism for the detection of a specific magnetic symmetry. The analysis of the hyperfine lines in the $g_{||,eff}$ provides useful information regarding the relative magnitude of the exchange coupling constants.[14] A similar methodology has been followed in the case of trinuclear [Fe_3] clusters by use of Mössbauer spectroscopy.[69] As a matter of fact, the analysis of the hyperfine interactions via such spectroscopic methods can reveal lower symmetries, which would require an overparameterization in the analysis of the usual magnetic measurements.

Here, in the case of isolated trinuclear clusters, EPR spectra are reported from powder samples. These spectra have provided compelling evidence for the significant role of the antisymmetric exchange interaction via the existence of a $g_{\perp,eff}$ << 2.0, as has been analyzed above. On the other hand, in the majority of the cases, the $g_{||,eff}$ region in the powder spectra does not show well resolved hyperfine lines and no attempts have been reported to analyze this part of the spectrum.[3,8,41–43] An exception to the above was the case of two trinuclear Cu_3 clusters whose crystal structures were determined at 213 K and 143 K,[70–72] respectively, revealing equilateral configurations. The conventional magnetic susceptibility measurements could be fitted with the isotropic exchange model in the equilateral symmetry without indication of lower symmetry. However, EPR measurements at liquid helium temperatures revealed hyperfine lines, the analysis of which indicated a lower than equilateral symmetry. While the physical origin of this effect has been postulated as a structural rearrangement[50,70] occurring at temperatures below those of crystal structure determinations (i.e. T < 100 K), also known as the "magnetic Jahn-Teller effect", the only available structural data point toward a dynamic symmetry decrease due to atomic vibrations.[52]

In the present case, well resolved hyperfine patterns are obtained in frozen solutions at liquid helium temperatures. The pattern readily indicates that the unpaired spin is localized mainly at a single Cu-center of the trinuclear unit. The dipolar model adopted to analyze the EPR spectra from the powder sample at liquid helium temperatures is also consistent with the spin being localized at one metal center of each trinuclear unit. As it has been discussed, both observations indicate that the exchange coupling scheme is consistent with the case of one strong and two weak exchange coupling constants. Following the description of Ferrer et al.,[3] the average of the two most similar Cu-O-Cu angles of **1** is β = 115.28°, whereas the third angle γ = 109.29°. Within the magnetostructural correlations, the relative magnitude of the angles β and γ suggest two large exchange coupling constants and one smaller ($|J|$ > $|j|$). More detailed theoretical calculations are needed to better understand the present discrepancy between the low temperature EPR spectroscopic data and the magnetostructural correlations.

There remains an open question regading the transmission of *inter*-molecular magnetic interactions through H-bonds, and the mechanism of their propagation. One plausible mechanism involves magnetic exchange – e.g. other authors have interpreted the magnetic susceptibility and EPR spectroscopic data of their H-bonded systems assuming an *inter*-molecular isotropic magnetic exchange transmitted via the H-bonds: A weak intermolecular antiferromagnetic exchange of -0.051 cm^{-1} was calculated to operate between H-bonded dinuclear Cu^{II} paddle-wheel complexes, and a ferromagnetic exchange of (0.19 - 0.39 cm^{-1}) was determined to propagate along a plane of an H-bonded organic radicals.[73,74] Weak intra- and inter-molecular exchange interactions (~0.22 cm^{-1}) have been identified in Fe^{III} Schiff-base complexes.[75]

In the present case, it has been clearly demonstrated that the main magnetic interaction is through the point dipole approximation. We have previously demonstrated a similar example with two H-bonded $\{Fe_3O\}^{7+}$ clusters interacting mainly through dipolar interactions as well.[76] The use of dipolar interactions for the structural elucidation of biological molecules has been well established, not only through CW EPR spectroscopy, but also through pulsed EPR techniques. For example, Double Electron Electron Resonance (DEER) and Pulsed Electron Double Resonance (PELDOR) have been routinely applied to systems with radical spins and/or mononuclear paramagnetic transition metal centers with localized spin densities. Our work here provides insights as to how such techniques can be applied to exchange-coupled systems, where the problem of spin localization is more complex, rendering the structural analysis of such systems possible.

Our work here also demonstrates the utility of H-bonds in the construction of weakly coupled systems for the development of molecular Quantum Information Processing devices. It has been demonstrated that H-bonded dimers of a Mn_4 SMM experience an exchange bias that modulates the quantum tunneling of their magnetization and couples them quantum mechanically, providing a mechanism to create coherent quantum superposition states (Christou ad Hill, Nature 2002, Science 2003). While the magnetic coupling mechanism (i.e. exchange interaction *vs*. dipolar) and the type of molecule (high-spin SMM *vs*. S = 1/2 triangle) are quite different from the one operating here in compound **1**, the possibility is quite intriguing. Further experiments should be designed to test the potential of this dimer to extend further the qubit encoding scheme previously examined by us[77] and others.[78, 79]

Conflicts of interest

There are no conflicts to declare.

Acknowledgements

LM, AKB and RGR acknowledge the financial support of the National Science Foundation (CHE-1213683) and the National Aeronautics and Space Administration (NNX13AD38A). M.P. and Y.S. acknowledge support by the project MIS 5002567, implemented under the "Action for the Strategic Development

on the Research and Technological Sector", funded by the Operational Programme "Competitiveness, Entrepreneurship and Innovation" (NSRF 2014-2020) and co-financed by Greece and the European Union (European Regional Development Fund). This project has received funding from the European Union's Horizon 2020 research and innovation programme under the Marie Sklodowska-Curie grant agreement No 746060 (for AKB and PT). The SpinCount software was kindly provided by Prof. M. P. Hendrich, Carnegie Mellon University, Pittsburgh, PA, U.S.A.

References

1 L.-L. Wang, Y.-M. Sun, Z.-Y. Yu, Z.-N. Qi and C.-B. Liu, *J. Phys. Chem. A*, 2009, **113**, 10534–10539.
2 S. Ferrer, F. Lloret, Bertomeu, Ignacio, Alzuet, Gloria, Borrás, Joaquín, García-Granda, Santiago, Liu-González, Malva and J. G. Haasnoot, .
3 S. Ferrer, F. Lloret, E. Pardo, J. M. Clemente-Juan, M. Liu-González and S. García-Granda, *Inorg. Chem.*, 2012, **51**, 985–1001.
4 R. Boča and R. Herchel, *Coord. Chem. Rev.*, 2010, **254**, 2973–3025.
5 E. I. Solomon, A. J. Augustine and J. Yoon, *Dalton Trans.*, 2008, 3921.
6 C. Pettinari, N. Masciocchi, L. Pandolfo and D. Pucci, *Chem. - Eur. J.*, 2010, **16**, 1106–1123.
7 A. Chakraborty, K. L. Gurunatha, A. Muthulakshmi, S. Dutta, S. K. Pati and T. K. Maji, *Dalton Trans.*, 2012, **41**, 5879.
8 A. Escuer, G. Vlahopoulou, F. Lloret and F. A. Mautner, *Eur. J. Inorg. Chem.*, 2014, **2014**, 83–92.
9 S. Carretta, P. Santini, G. Amoretti, F. Troiani and M. Affronte, *Phys. Rev. B*, 2007, **76**, 024408.
10 S.-K. Lee, S. D. George, W. E. Antholine, B. Hedman, K. O. Hodgson and E. I. Solomon, *J. Am. Chem. Soc.*, 2002, **124**, 6180–6193.
11 J. Yoon and E. I. Solomon, *Coord. Chem. Rev.*, 2007, **251**, 379–400.
12 E. I. Solomon, U. M. Sundaram and T. E. Machonkin, *Chem. Rev.*, 1996, **96**, 2563–2606.
13 E. I. Solomon, M. J. Baldwin and M. D. Lowery, *Chem. Rev.*, 1992, **92**, 521–542.
14 M. I. Belinsky, *Inorg. Chem.*, 2004, **43**, 739–746.
15 M. I. Belinsky, *Inorg. Chem.*, 2008, **47**, 3532–3539.
16 M. I. Belinsky, *Inorg. Chem.*, 2008, **47**, 3521–3531.
17 M. Trif, F. Troiani, D. Stepanenko and D. Loss, *Phys. Rev. B*, 2010, **82**, 045429.
18 M. Trif, F. Troiani, D. Stepanenko and D. Loss, *Phys. Rev. Lett.*, 2008, **101**, 217201.
19 F. Troiani, D. Stepanenko and D. Loss, *Phys. Rev. B*, 2012, **86**, 161409(R).
20 R. Boča, L. Dlháň, G. Mezei, T. Ortiz-Pérez, R. G. Raptis and J. Telser, *Inorg. Chem.*, 2003, **42**, 5801–5803.
21 E. M. Zueva, M. M. Petrova, R. Herchel, Z. Trávníček, R. G. Raptis, L. Mathivathanan and J. E. McGrady, *Dalton Trans.*, 2009, 5924.
22 P. A. Angaridis, P. Baran, R. Boča, F. Cervantes-Lee, W. Haase, G. Mezei, R. G. Raptis and R. Werner, *Inorg. Chem.*, 2002, **41**, 2219–2228.
23 G. Mezei, R. G. Raptis and J. Telser, *Inorg. Chem.*, 2006, **45**, 8841–8843.
24 G. Mezei, M. Rivera-Carrillo and R. G. Raptis, *Dalton Trans*, 2007, 37–40.
25 W. L. F. Armarego and C. L. L. Chai, *Purification of laboratory chemicals*, Butterworth-Heinemann, Amsterdam ; Boston, 5th ed., 2003.
26 N. F. Chilton, R. P. Anderson, L. D. Turner, A. Soncini and K. S. Murray, *J. Comput. Chem.*, 2013, **34**, 1164–1175.
27 S. Stoll and A. Schweiger, *J. Magn. Reson.*, 2006, **178**, 42–55.
28 Bruker, *SAINT, APEX3, SADABS*, Bruker AXS Inc., Madison, Wisconsin, USA, 2016.
29 G. M. Sheldrick, *Acta Crystallogr. Sect. C Struct. Chem.*, 2015, **71**, 3–8.
30 O. V. Dolomanov, L. J. Bourhis, R. J. Gildea, J. A. K. Howard and H. Puschmann, *J. Appl. Crystallogr.*, 2009, **42**, 339–341.
31 B. M. Ahmed and G. Mezei, *Inorg. Chem.*, 2016, **55**, 7717–7728.
32 A. Alsalme, M. Ghazzali, R. A. Khan, K. Al-Farhan and J. Reedijk, *Polyhedron*, 2014, **75**, 64–67.
33 F. B. Hulsbergen, R. W. M. ten Hoedt, G. C. Verschoor, J. Reedijk and A. L. Spek, *J. Chem. Soc. Dalton Trans.*, 1983, 539–545.
34 C. Di Nicola, F. Garau, M. Gazzano, M. Monari, L. Pandolfo, C. Pettinari and R. Pettinari, *Cryst. Growth Des.*, 2010, **10**, 3120–3131.
35 S. Carlotto, M. Casarin, A. Lanza, F. Nestola, L. Pandolfo, C. Pettinari and R. Scatena, *Cryst. Growth Des.*, 2015, **15**, 5910–5918.
36 Y. Agnus, R. Louis, B. Metz, C. Boudon, J. P. Gisselbrecht and M. Gross, *Inorg. Chem.*, 1991, **30**, 3155–3161.
37 S. Ferrer, J. G. Haasnoot, J. Reedijk, E. Müller, M. Biagini Cingi, M. Lanfranchi, A. M. Manotti Lanfredi and J. Ribas, *Inorg. Chem.*, 2000, **39**, 1859–1867.
38 L. K. Das, M. G. B. Drew, C. Diaz and A. Ghosh, *Dalton Trans.*, 2014, **43**, 7589.
39 J. S. Costa, N. A. G. Bandeira, B. Le Guennic, V. Robert, P. Gamez, G. Chastanet, L. Ortiz-Frade and L. Gasque, *Inorg. Chem.*, 2011, **50**, 5696–5705.
40 S. Karmakar, O. Das, S. Ghosh, E. Zangrando, M. Johann, E. Rentschler, T. Weyhermüller, S. Khanra and T. Kanti Paine, *Dalton Trans.*, 2010, **39**, 10920.
41 X. Liu, M. P. de Miranda, E. J. L. McInnes, C. A. Kilner and M. A. Halcrow, *Dalton Trans.*, 2004, 59–64.
42 T. C. Stamatatos, J. C. Vlahopoulou, Y. Sanakis, C. P. Raptopoulou, V. Psycharis, A. K. Boudalis and S. P. Perlepes, *Inorg. Chem. Commun.*, 2006, **9**, 814–818.
43 T. Afrati, C. Dendrinou-Samara, C. Raptopoulou, A. Terzis, V. Tangoulis and D. P. Kessissoglou, *Dalton Trans.*, 2007, 5156–5164.
44 S. Speed, M. Font-Bardía, M. S. E. Fallah and R. Vicente, *Dalton Trans.*, 2014, **43**, 16919–16927.
45 T. Afrati, C. Dendrinou-Samara, C. Raptopoulou, A. Terzis, V. Tangoulis, A. Tsipis and D. P. Kessissoglou, *Inorg. Chem.*, 2008, **47**, 7545–7555.
46 T. Murao, *Phys. Lett. A*, 1974, **49**, 33–35.
47 A. K. Boudalis, Y. Sanakis, F. Dahan, M. Hendrich and J.-P. Tuchagues, *Inorg. Chem.*, 2006, **45**, 443–453.
48 V. Psycharis, C. P. Raptopoulou, A. K. Boudalis, Y. Sanakis, M. Fardis, G. Diamantopoulos and G. Papavassiliou, *Eur. J. Inorg. Chem.*, 2006, **2006**, 3710–3723.
49 Y. Sanakis, A. L. Macedo, I. Moura, J. J. G. Moura, V. Papaefthymiou and E. Münck, *J. Am. Chem. Soc.*, 2000, **122**, 11855–11863.

50 J. Yoon, L. M. Mirica, T. D. P. Stack and E. I. Solomon, *J. Am. Chem. Soc.*, 2004, **126**, 12586–12595.
51 H. De Raedt, S. Miyashita, K. Michielsen and M. Machida, *Phys. Rev. B*, , DOI:10.1103/PhysRevB.70.064401.
52 A. N. Georgopoulou, I. Margiolaki, V. Psycharis and A. K. Boudalis, *Inorg. Chem.*, 2017, **56**, 762–772.
53 D. H. Jones, J. R. Sams and R. C. Thompson, *J. Chem. Phys.*, 1984, **81**, 440–447.
54 A. N. Georgopoulou, Y. Sanakis and A. K. Boudalis, *Dalton Trans.*, 2011, **40**, 6371–6374.
55 Y. V. Rakitin, Y. V. Yablokov and V. V. Zelentsov, *J. Magn. Reson.*, 1981, **43**, 288–301.
56 D. Piñero, P. Baran, R. Boca, R. Herchel, M. Klein, R. G. Raptis, F. Renz and Y. Sanakis, *Inorg. Chem.*, 2007, **46**, 10981–10989.
57 V. Rabe, W. Frey, A. Baro, S. Laschat, M. Bauer, H. Bertagnolli, S. Rajagopalan, T. Asthalter, E. Roduner, H. Dilger, T. Glaser and D. Schnieders, *Eur. J. Inorg. Chem.*, 2009, **2009**, 4660–4674.
58 A. Vlachos, V. Psycharis, C. P. Raptopoulou, N. Lalioti, Y. Sanakis, G. Diamantopoulos, M. Fardis, M. Karayanni, G. Papavassiliou and A. Terzis, *Inorganica Chim. Acta*, 2004, **357**, 3162–3172.
59 A. Bencini, D. Gatteschi and A. Bencini, *EPR of exchange coupled systems*, Dover Publications, Inc, Mineola, N.Y, Dover ed., 2012.
60 X. Liu, J. A. McAllister, M. P. de Miranda, E. J. L. McInnes, C. A. Kilner and M. A. Halcrow, *Chem. – Eur. J.*, 2004, **10**, 1827–1837.
61 J. R. Pilbrow, *Transition ion electron paramagnetic resonance*, Clarendon Press ; Oxford University Press, Oxford : New York, 1990.
62 B. Bennett, W. E. Antholine, V. M. D'souza, G. Chen, L. Ustinyuk and R. C. Holz, *J. Am. Chem. Soc.*, 2002, **124**, 13025–13034.
63 W. Rammal, C. Belle, C. Béguin, C. Duboc, C. Philouze, J.-L. Pierre, L. Le Pape, S. Bertaina, E. Saint-Aman and S. Torelli, *Inorg. Chem.*, 2006, **45**, 10355–10362.
64 A. Galani, E. K. Efthimiadou, G. Mitrikas, Y. Sanakis, V. Psycharis, C. Raptopoulou, G. Kordas and A. Karaliota, *Inorganica Chim. Acta*, 2014, **423**, 207–218.
65 T. D. Smith and J. R. Pilbrow, *Coord. Chem. Rev.*, 1974, **13**, 173–278.
66 R. E. Coffman and G. R. Buettner, *J. Phys. Chem.*, 1979, **83**, 2392–2400.
67 P. Bertrand, C. More, B. Guigliarelli, A. Fournel, B. Bennett and B. Howes, *J. Am. Chem. Soc.*, 1994, **116**, 3078–3086.
68 Elsässer, Celine, Brecht, Marc and Bittl, Robert, *J. Am. Chem. Soc.*, 2002, **124**, 12606–12611.
69 T. A. Kent, B. H. Huynh and E. Münck, *Proc. Natl. Acad. Sci.*, 1980, **77**, 6574–6576.
70 B. Cage, F. A. Cotton, N. S. Dalal, E. A. Hillard, B. Rakvin and C. M. Ramsey, *J. Am. Chem. Soc.*, 2003, **125**, 5270–5271.
71 R. Clérac, F. A. Cotton, K. R. Dunbar, E. A. Hillard, M. A. Petrukhina and B. W. Smucker, *Comptes Rendus Académie Sci. - Ser. IIC - Chem.*, 2001, **4**, 315–319.
72 L. M. Mirica and T. D. P. Stack, *Inorg. Chem.*, 2005, **44**, 2131–2133.
73 V. Paredes-García, R. C. Santana, R. Madrid, A. Vega, E. Spodine and D. Venegas-Yazigi, *Inorg. Chem.*, 2013, **52**, 8369–8377.
74 J. Cirujeda, E. Hernàndez-Gasió, C. Rovira, J.-L. Stanger, P. Turek and J. Veciana, *J Mater Chem*, 1995, **5**, 243–252.
75 R. Herchel, I. Nemec, M. Machata and Z. Trávníček, *Inorg. Chem.*, 2015, **54**, 8625–8638.
76 A. K. Boudalis, Y. Sanakis, C. P. Raptopoulou, A. Terzis, J.-P. Tuchagues and S. P. Perlepes, *Polyhedron*, 2005, **24**, 1540–1548.
77 G. Mitrikas, Y. Sanakis, C. P. Raptopoulou, G. Kordas, G. Papavassiliou, *Phys. Chem. Chem. Phys.*, 2008, **10**, 743–748.
78 S. Bertaina, S. Gambarelli, T. Mitra, B. Tsukerblat, A. Müller, B. Barbara, *Nature*, 2008, **453**, 203–206.
79 P. Lutz, R. Marx, D. Dengler, A. Kromer, J. van Slageren, *Mol. Phys.*, 2013, **111**, 2897–2902.